Journal of Robotics and Control (JRC)
Volume 5, Issue 6, 2024
ISSN: 2715-5072, DOI: 10.18196/jrc.v5i6.23074

Landing Control Based on Energy Prediction for a Quadcopter Under External Disturbances

Cuong V. Nguyen [1*]
[1] Thai Nguyen University of Information and Communication Technology (ICTU), Viet Nam
Email: [1] nvcuong@ictu.edu.vn
*Corresponding Author

***Abstract*—Unmanned aerial vehicles (UAVs) have recently become one of the most popular research topics. The high diversity in its uses has attracted research attention regarding structure or control capabilities. However, if the energy consumed in each mission cannot be predicted, the available flight time will pose many risks to the UAV and data security. This paper proposes a control algorithm based on predicting the remaining flight time to determine a safe landing station. Suppose the UAV cannot reach the desired destination station. In that case, it will find the nearest landing station to recharge its energy until the SoC (State of Charge) > 90%, then the UAV will continue to perform the mission until the UAV reaches the destination station. In addition, the paper uses a marker-based landing method to improve landing accuracy. The sliding mode controller (SMC) is designed to consider external disturbance factors and consider a solution to reduce chattering.**

Keywords—SMC; UAV; Control; Landing; Energy Prediction.

I. INTRODUCTION

In recent years, the research of unmanned aerial vehicles (UAVs) for civil or military applications has promoted the need to operate these systems with higher requirements. The UAVs have shown versatility as well as efficiency in various fields such as search and rescue (SAR) [1][2], meteorological research [3]-[6], infrastructure testing [7]-[10], homeland security and traffic monitoring [11]-[15], and precision agriculture [16]-[20]. With a large number of quadcopters in use, it is undeniable that quadcopters are capable of because of their convenience and flexibility in narrow operating ranges. They can fly in low areas, hover, and provide detailed information about that area through the control station [21][22].

Unmanned aerial vehicles (UAVs) in the form of quadcopters are a popular research topic. The ability to perform various aerial maneuvers opens up many opportunities for creating applications such as surveillance systems, delivery, video recording, or other military purposes. However, the success rate of such applications depends on the flight time in relation to energy consumption and battery capacity [23]-[25].

UAVs (Unmanned Aerial Vehicles), also known as drones, can encounter many serious risks when operating and encountering a situation where the battery runs out [26]. Here are some of the main risks:

Free fall: If the UAV's battery suddenly runs out, it can completely lose control and fall freely, causing damage to the UAV, property, or people below.

Loss of control: A weak battery can cause the UAV to lose its ability to maintain stability and control, leading to uncontrolled movement and the risk of collision with other objects.

Data loss: If the UAV is performing a recording or data collection mission, a sudden battery drain can cause the loss of data that has not been stored yet.

Economic Loss: A crashed or damaged UAV can result in high repair or replacement costs, affecting the economic viability of the missions the UAV is performing.

Therefore, proper battery testing and management, as well as using the PIN SoC monitoring and prediction system to issue emergency landing control commands, are essential to minimize risks.

There are many methods to control a quadcopter to follow a given trajectory such as the PID method [27]-[30]. In the article [31]-[35], the author proposes a Backstepping controller to control the position and attitude of the quadcopter. The sliding control method is one of the popular methods used to control a quadcopter as presented in the article [36]-[41]. In the article [42]-[45], the author uses neural network method combined with other methods to build a quadcopter controller. However, this method requires a huge computing capacity. Linear controllers such as PID and LQR are not good for controlling a strongly nonlinear object like a quadcopter. In this article we build an SMC controller to control a quadcopter to follow a trajectory and land based on energy prediction.

The landing phase is the last and most important phase of a UAV's navigation process [46]. Therefore, landing methods for UAVs are attracting considerable attention from researchers worldwide. Previous studies have proposed global positioning systems (GPS) and inertial navigation sensors (INS) as the main positioning systems [47]-[49]. However, data from the GPS often has large deviations. Therefore, the landing location is often 1 to 3 m from the desired location [50]. Based on the above issues, this work aims to develop a new marker-based landing system that uses a sliding mode control to control the UAV's trajectory and land in a specific location with great precision. The landing position error of the UAV has been improved thanks to the use of ArUco markers [51]-[58].

Research and development of methods to determine optimal landing points based on the remaining battery SoC for quadcopters is a topic that is attracting the attention of many researchers around the world. In [59], the authors studied an energy-saving landing planning method for UAVs based on SoC and wind speed predictions, determining the optimal quadcopter landing trajectory under changing weather conditions. In [60], the authors studied how to select the optimal landing point for quadcopters based on the remaining SoC of the battery and ground obstacles. In [61][62], the authors focused on optimal trajectory planning and energy saving for quadcopters during landing. In [63][64], an overview of the methods and challenges in energy-saving flight for quadcopters, including SoC-based landing planning.

The contribution of this paper is given by the following points: i) Building an SMC controller based on Lyapunov stability theory considers external disturbances. ii) Building a flight and landing algorithm based on real-time energy consumption prediction of the quadcopter, thereby creating a basis for building a control scheme in different modes. That has helped the quadcopter avoid risks such as collision with stations, loss, etc., and supported the quadcopter in operating more effectively. iii)The UAV's landing process is based on the marker maker instead of using the signal sent back from the GPS system, so the accuracy is significantly improved during the experiment [65]-[67].

The rest of this paper is organized as follows. The kinematic model of the Quadcopter is presented in Section 2. The SMC for position control and attitude control is described in Section 3. Landing control based on energy prediction shown in Section 4. Finally, conclusions are provided in Section 5.

II. DYNAMIC MODELLING FOR A QUADCOPTER

The structural model of the quadrotor and the coordinate systems used in building the dynamics model of the quadrotor are shown in Fig. 1.

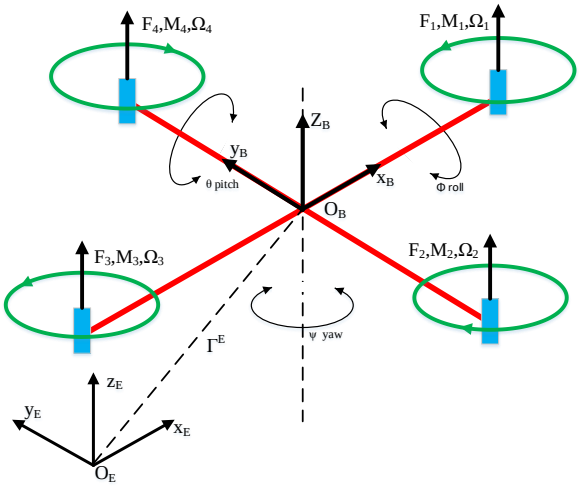

Fig. 1. Structural model of Quadrotor

Using the Newton - Euler method for the model [68], we get the quadrotor's equations of motion as (1).

$$\begin{cases} m\ddot{\Gamma}^E = F_{th} - F_d - F_g - F_n \\ I\ddot{\Theta}^E = M - M_{gp} - M_{gb} - M_n \end{cases} \quad (1)$$

where $F_{th} = R_\Theta(\phi,\theta,\psi)[0,0\sum_{i=1}^{4} F_i]^T$ is the total thrust of the four propellers; $F_d = diag(k_1,k_2,k_3)\dot{\Gamma}^T$ is the air resistance against the quadcopter's motion; $F_g = [0,0,mg]^T$ is the force of gravity; F_n is the total resistance of the noise types not included in the above components. $M = [M_\phi, M_\theta, M_\psi]^T$ is the sum of the moments of the roll, pitch, and yaw angles; M_{gp} and M_{gb} are the gyroscope moments; M_n is the resisting moment component of the disturbance, not included in the above components; k_1, k_2, and k_3 are drag coefficients.

Substituting the position vector and force components into expression (1), we get the quadcopter's translational dynamics equation as (2).

$$\begin{cases} \ddot{x} = -\frac{k_x}{m}\dot{x} + (cos\emptyset sin\theta cos\psi + sin\emptyset sin\psi)\frac{U_1}{m} - \frac{F_{nx}}{m} \\ \ddot{y} = -\frac{k_y}{m}\dot{y} + (cos\emptyset sin\theta sin\psi + sin\emptyset cos\psi)\frac{U_1}{m} - \frac{F_{ny}}{m} \\ \ddot{z} = -\frac{k_z}{m}\dot{z} - g + (cos\emptyset cos\theta)\frac{U_1}{m} - \frac{F_{nz}}{m} \end{cases} \quad (2)$$

where F_{nx}, F_{ny}, F_{nz} are the repulsive forces of the disturbance in the x, y, and z directions. Substituting the moment components into Equation (2) of (1), we get the kinematics equation for the rotation of the quadcopter as (3).

$$\begin{cases} \ddot{\emptyset} = \dot{\theta}\dot{\psi}\frac{I_y - I_z}{I_x} - \frac{J_p}{I_x}\Omega_\Sigma\dot{\theta} + lb\frac{U_2}{I_x} - \frac{M_{n\emptyset}}{I_x} \\ \ddot{\theta} = \dot{\emptyset}\dot{\psi}\frac{I_z - I_x}{I_y} + \frac{J_p}{I_y}\Omega_\Sigma\dot{\emptyset} + lb\frac{U_3}{I_y} - \frac{M_{n\theta}}{I_y} \\ \ddot{\psi} = \dot{\emptyset}\dot{\theta}\frac{I_x - I_y}{I_z} + d\frac{U_4}{I_z} - \frac{M_{n\psi}}{I_z} \end{cases} \quad (3)$$

where $\Omega_\Sigma = \Omega_1 - \Omega_2 + \Omega_3 - \Omega_4$ is the total speed of the propellers; $M_{n\emptyset}, M_{n\theta}, M_{n\psi}$ are the resisting moment components of the disturbance acting on the roll, pitch, and yaw angles. The complete system of kinetic equations of the Quadcopter in the presence of external disturbances is expressed as (4).

$$\begin{cases} \ddot{x} = -\frac{k_x}{m}\dot{x} + (cos\emptyset sin\theta cos\psi + sin\emptyset sin\psi)\frac{U_1}{m} - \frac{F_{nx}}{m} \\ \ddot{y} = -\frac{k_y}{m}\dot{y} + (cos\emptyset sin\theta sin\psi + sin\emptyset cos\psi)\frac{U_1}{m} - \frac{F_{ny}}{m} \\ \ddot{z} = -\frac{k_z}{m}\dot{z} - g + (cos\emptyset cos\theta)\frac{U_1}{m} - \frac{F_{nz}}{m} \\ \ddot{\emptyset} = \dot{\theta}\dot{\psi}\frac{I_y - I_z}{I_x} - \frac{J_p}{I_x}\Omega_\Sigma\dot{\theta} + lb\frac{U_2}{I_x} - \frac{M_{n\emptyset}}{I_x} \\ \ddot{\theta} = \dot{\emptyset}\dot{\psi}\frac{I_z - I_x}{I_y} + \frac{J_p}{I_y}\Omega_\Sigma\dot{\emptyset} + lb\frac{U_3}{I_y} - \frac{M_{n\theta}}{I_y} \\ \ddot{\psi} = \dot{\emptyset}\dot{\theta}\frac{I_x - I_y}{I_z} + d\frac{U_4}{I_z} - \frac{M_{n\psi}}{I_z} \end{cases} \quad (4)$$

We let $X^T = (x,y,z,\dot{x},\dot{y},\dot{z},\phi,\theta,\psi,\dot{\phi},\dot{\theta},\dot{\psi})^T$ be the vector of state variables. The input is the propeller speed given by the equation (5).

$$\begin{cases} U_1 = b(\Omega_1^2 + \Omega_2^2 + \Omega_3^2 + \Omega_4^2) \\ U_2 = lb(-\Omega_2^2 + \Omega_4^2) \\ U_3 = lb(-\Omega_1^2 + \Omega_3^2) \\ U_4 = d(\Omega_1^2 - \Omega_2^2 + \Omega_3^2 - \Omega_4^2) \\ \Omega_\Sigma = \Omega 1 - \Omega 2 + \Omega 3 - \Omega 4 \end{cases} \quad (5)$$

The equation of state describing the kinematics of the quadcopter has the following form (6)

$$\begin{cases} \dot{x}_1 = x_2 \\ \dot{x}_2 = -\frac{k_x}{m}\dot{x} + (cos\emptyset sin\theta cos\psi + sin\emptyset sin\psi)\frac{U_1}{m} - \frac{F_{nx}}{m} \\ \dot{x}_3 = x_4 \\ \dot{x}_4 = -\frac{k_y}{m}\dot{y} + (cos\emptyset sin\theta sin\psi + sin\emptyset cos\psi)\frac{U_1}{m} - \frac{F_{ny}}{m} \\ \dot{x}_5 = x_6 \\ \dot{x}_6 = -\frac{k_z}{m}\dot{z} - g + (cos\emptyset cos\theta)\frac{U_1}{m} - \frac{F_{nz}}{m} \\ \dot{x}_7 = x_8 \\ \dot{x}_8 = \dot{\theta}\dot{\psi}\frac{I_y - I_z}{I_x} - \frac{J_p}{I_x}\Omega_\Sigma\dot{\theta} + lb\frac{U_2}{I_x} - \frac{M_{n\emptyset}}{I_x} \\ \dot{x}_9 = x_{10} \\ \dot{x}_{10} = \dot{\emptyset}\dot{\psi}\frac{I_z - I_x}{I_y} + \frac{J_p}{I_y}\Omega_\Sigma\dot{\emptyset} + lb\frac{U_3}{I_y} - \frac{M_{n\theta}}{I_y} \\ \dot{x}_{11} = x_{12} \\ \dot{x}_{12} = \dot{\emptyset}\dot{\theta}\frac{I_x - I_y}{I_z} + \frac{dU_4}{I_z} - \frac{M_{n\psi}}{I_z} \end{cases} \quad (6)$$

From the system of equations of state of Quadcopter (6) we set:

$h_1 = -\frac{k_x}{m}; h_2 = -\frac{F_{nx}}{m}; h_3 = -\frac{k_y}{m}; h_4 = -\frac{F_{ny}}{m}; \ h_5 = -\frac{k_z}{m}; \ h_6 = -\frac{F_{nz}}{m}; \ h_7 = \frac{I_y - I_z}{I_x}; \ h_8 = -\frac{J_r}{I_x}\Omega_\Sigma; \ h_9 = lb\frac{1}{I_x}; \ h_{10} = -\frac{M_{n\emptyset}}{I_x}; h_{11} = \frac{I_z - I_x}{I_y}; \ h_{12} = \frac{J_p}{I_y}\Omega_\Sigma; \ h_{13} = \frac{lb}{I_y}; \ h_{14} = -\frac{M_{n\theta}}{I_y}; \ h_{15} = \frac{I_x - I_y}{I_z}; \ h_{16} = \frac{d}{I_z}; h_{17} = -\frac{M_{n\psi}}{I_z}; \ \Omega_\Sigma = \omega_1 - \omega_2 + \omega_3 - \omega_4;$

$U_x = \frac{U_1}{m}(cos\emptyset sin\theta cos\psi + sin\emptyset sin\psi); U_z = \frac{U_1}{m}(cos\emptyset cos\theta) - g;$

$U_y = \frac{U_1}{m}(cos\emptyset sin\theta sin\psi + sin\emptyset cos\psi);$

Then equation (6) is rewritten as (7).

$$\begin{cases} \dot{x}_1 = x_2 \\ \dot{x}_2 = h_1 x_2 + h_2 + U_x \\ \dot{x}_3 = x_4 \\ \dot{x}_4 = h_3 x_4 + h_4 + U_y \\ \dot{x}_5 = x_6 \\ \dot{x}_6 = h_5 x_6 + h_6 + U_z \\ \dot{x}_7 = x_8 \\ \dot{x}_8 = h_7 x_{10} x_{12} + h_8 x_{10} + h_{10} + h_9 U_2 \\ \dot{x}_9 = x_{10} \\ \dot{x}_{10} = h_{11} x_8 x_{12} + h_{12} x_8 + h_{14} + h_{13} U_3 \\ \dot{x}_{11} = x_{10} \\ \dot{x}_{12} = h_{15} x_8 x_{10} + h_{17} + h_{16} U_4 \end{cases} \quad (7)$$

III. CONTROLLER DESIGN FOR QUADCOPTER

In this section, we have built a control scheme to control the position and attitude of the quadcopter using SMC. Position and attitude controllers were constructed, and the stability of the proposed controller was also proven.

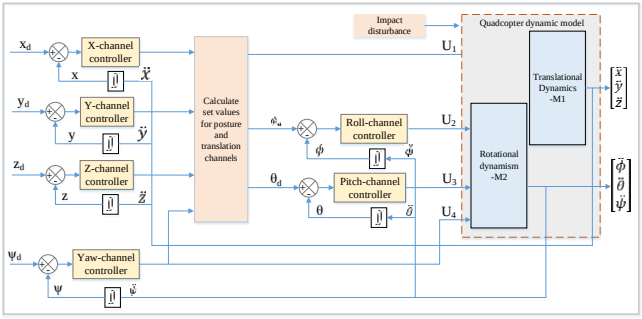

Fig. 2. Block diagram of the quadcopter channel control system

A. *Sliding Mode Controller Design for Position Attitude Control Quadcopter.*

We set the tracking error:

$$\begin{bmatrix} e_1 \\ e_3 \\ e_5 \end{bmatrix} = \begin{bmatrix} x_1 - x_{1d} \\ x_3 - x_{3d} \\ x_5 - x_{5d} \end{bmatrix} \Rightarrow \begin{bmatrix} \dot{e_1} \\ \dot{e_3} \\ \dot{e_5} \end{bmatrix} = \begin{bmatrix} \dot{x_1} - \dot{x_{1d}} \\ \dot{x_3} - \dot{x_{3d}} \\ \dot{x_5} - \dot{x_{5d}} \end{bmatrix} = \begin{bmatrix} x_2 - \dot{x_{1d}} \\ x_4 - \dot{x_{3d}} \\ x_6 - \dot{x_{5d}} \end{bmatrix} \quad (8)$$

Select the sliding surface as follows:

$$s = \begin{bmatrix} s_1 \\ s_3 \\ s_5 \end{bmatrix} = \begin{bmatrix} c_1 e_1 + c_2 \dot{e_1} \\ c_3 e_3 + c_4 \dot{e_3} \\ c_5 e_5 + c_6 \dot{e_5} \end{bmatrix} \Rightarrow$$

$$\dot{s} = \begin{bmatrix} c_1 \dot{e_1} + c_2 \ddot{e_1} \\ c_3 \dot{e_3} + c_4 \ddot{e_3} \\ c_5 \dot{e_5} + c_6 \ddot{e_5} \end{bmatrix} = \begin{bmatrix} c_1(x_2 - \dot{x_{1d}}) + c_2(\dot{x_2} - \ddot{x_{1d}}) \\ c_3(x_4 - \dot{x_{3d}}) + c_4(\dot{x_4} - \ddot{x_{3d}}) \\ c_5(x_6 - \dot{x_{5d}}) + c_6(\dot{x_6} - \ddot{x_{5d}}) \end{bmatrix} \quad (9)$$

Substituting $\dot{x_2}, \dot{x_4}, \dot{x_6}$ into equation (9), we have:

$$\dot{s} = \begin{bmatrix} c_1(x_2 - \dot{x_{1d}}) + c_2(h_1 x_2 + h_2 + U_x - \ddot{x_{1d}}) \\ c_3(x_4 - \dot{x_{3d}}) + c_4(h_3 x_4 + h_4 + U_y - \ddot{x_{3d}}) \\ c_5(x_6 - \dot{x_{5d}}) + c_6(h_5 x_6 + h_6 + U_z - \ddot{x_{5d}}) \end{bmatrix} \quad (10)$$

Select the slide mode controller for the system. In the sliding mode controller, there are two components, which are equilibrium and robust terms, with the formula:

$$u = u_{EQ} + u_R \quad (11)$$

The equilibrium component will be selected by setting the sliding surface's derivative $\dot{s} = -ks$ and giving the system's uncertainty parameter = 0. Then we have:

$$\begin{bmatrix} u_{EQx} \\ u_{EQy} \\ u_{EQz} \end{bmatrix} = \begin{bmatrix} \frac{1}{c_2}(-c_1(x_2 - \dot{x_{1d}}) - c_2(h_1 x_2 - \ddot{x_{1d}}) - k_1 s_1) \\ \frac{1}{c_4}(-c_3(x_4 - \dot{x_{3d}}) - c_4(h_3 x_4 - \ddot{x_{3d}}) - k_3 s_3) \\ \frac{1}{c_6}(-c_5(x_6 - \dot{x_{5d}}) + c_6(h_5 x_6 - \ddot{x_{5d}}) - k_5 s_5) \end{bmatrix} \quad (12)$$

The robust component will be chosen $u_R = -\eta sign(s)$, so we have:

$$u_R = \begin{bmatrix} u_{Rx} \\ u_{Ry} \\ u_{Rz} \end{bmatrix} = \begin{bmatrix} -\frac{1}{c_2}(\eta_1 sign(s_1)) \\ -\frac{1}{c_4}(\eta_3 sign(s_3)) \\ -\frac{1}{c_6}(\eta_5 sign(s_5)) \end{bmatrix} \quad (13)$$

η is chosen so that $\eta \geq$ is the maximum value of the uncertain parameters in the system.

Substituting $u_{EQ}; u_R$ into (11) we have:

$$\begin{bmatrix} U_x \\ U_y \\ U_z \end{bmatrix} = \begin{bmatrix} \frac{1}{c_2}(-c_1(x_2 - \dot{x_{1d}}) - c_2(h_1 x_2 - \ddot{x_{1d}}) - k_1 s_1 - \eta_1 sign(s_1)) \\ \frac{1}{c_4}(-c_3(x_4 - \dot{x_{3d}}) - c_4(h_3 x_4 - \ddot{x_{3d}}) - k_3 s_3 - \eta_3 sign(s_3)) \\ \frac{1}{c_6}(-c_5(x_6 - \dot{x_{5d}}) + c_6(h_5 x_6 - \ddot{x_{5d}}) - k_5 s_5 - \eta_5 sign(s_5)) \end{bmatrix} \quad (14)$$

After obtaining the control signals U_x, U_y, U_z we calculate the control signal U_1 in the system of equations as follows:

$$U_1 = m\sqrt{U_x^2 + U_y^2 + (U_z + g)^2} \quad (15)$$

Prove stability of the controlled system.

Substituting the sliding mode control rule in expression (11) into (10), we have:

$$\dot{s} = \begin{bmatrix} \dot{s}_1 \\ \dot{s}_3 \\ \dot{s}_5 \end{bmatrix} = \begin{bmatrix} -k_1 s_1 - \eta_1 sign(s_1) + h_2 \\ -k_3 s_3 - \eta_3 sign(s_3) + h_4 \\ -k_5 s_5 - \eta_5 sign(s_5) + h_6 \end{bmatrix} \quad (16)$$

To prove the stability of the control system, the Lyapunov function is chosen as follows:

$$v = \begin{bmatrix} v_1 \\ v_3 \\ v_5 \end{bmatrix} = \begin{bmatrix} \frac{1}{2}s_1^2 \\ \frac{1}{2}s_3^2 \\ \frac{1}{2}s_5^2 \end{bmatrix} \quad (17)$$

Calculating the derivative v, we have:

$$\begin{bmatrix} \dot{v_1} \\ \dot{v_3} \\ \dot{v_5} \end{bmatrix} = \begin{bmatrix} s_1\dot{s_1} \\ s_3\dot{s_3} \\ s_5\dot{s_5} \end{bmatrix} = \begin{bmatrix} s_1(-k_1 s_1 - \eta_1 sign(s_1) + h_2) \\ s_3(-k_3 s_3 - \eta_3 sign(s_3) + h_4) \\ s_5(-k_5 s_5 - \eta_5 sign(s_5) + h_6) \end{bmatrix} = \begin{bmatrix} -k_1 s_1^2 - s_1(\eta_1 sign(s_1) - h_2) \\ -k_3 s_3^2 - s_3(\eta_3 sign(s_3) - h_4) \\ -k_5 s_5^2 - s_5(\eta_5 sign(s_5) - h_6) \end{bmatrix} \quad (18)$$

We have:

$$\begin{bmatrix} -k_1 s_1^2 - s_1(\eta_1 sign(s_1) - h_2) \\ -k_3 s_3^2 - s_3(\eta_3 sign(s_3) - h_4) \\ -k_5 s_5^2 - s_5(\eta_5 sign(s_5) - h_6) \end{bmatrix} \leq \begin{bmatrix} -k_1 s_1^2 - |s_1|(\eta_1 - h_2) \\ -k_3 s_3^2 - |s_3|(\eta_3 - h_4) \\ -k_5 s_5^2 - |s_5|(\eta_5 - h_6) \end{bmatrix} \leq \begin{bmatrix} -k_1 s_1^2 \\ -k_3 s_3^2 \\ -k_5 s_5^2 \end{bmatrix} \leq 0$$

Since we have the condition η. The η is chosen so that $\eta \geq$ is the maximum value of the uncertain parameters in the system. Therefore, according to the Lyapunov stability theory, our system is stable. The calculation process is similar to above, we have:

$$\begin{bmatrix} U_2 \\ U_3 \\ U_4 \end{bmatrix} = \begin{bmatrix} \frac{1}{c_8 h_9}[-c_7(x_8 - \dot{x_{7d}}) - c_8(h_7 x_{10} x_{12} + h_8 x_{10} - \ddot{x_{7d}}) - k_7 s_7 - \eta_7 sign(s_7)] \\ \frac{1}{c_{10} h_{13}}[-c_9(x_{10} - \dot{x_{9d}}) - c_{10}(h_{11} x_8 x_{12} + h_{12} x_8 - \ddot{x_{9d}}) - k_9 s_9 - \eta_9 sign(s_9)] \\ \frac{1}{c_{12} h_{16}}[-c_{11}(x_{12} - \dot{x_{11d}}) - c_{12}(h_{15} x_8 x_{10} - \ddot{x_{11d}}) - k_{11} s_{11} - \eta_{11} sign(s_{11})] \end{bmatrix} \quad (19)$$

B. Reduce Chattering Phenomenon

Sliding mode control (SMC) has several advantages: robustness against uncertainties and disturbances, high accuracy, finite-time convergence, and simplicity. However, sliding mode control has the disadvantage of the chattering phenomenon because it uses the ηsign(s) function in the control signal. Therefore, we need to devise a solution to overcome this phenomenon. In this study, we replace the ηsign(s) function with $\eta|s|^{\lambda}$sign(s). The simulation results in Fig. 3 demonstrate the effectiveness of this solution.

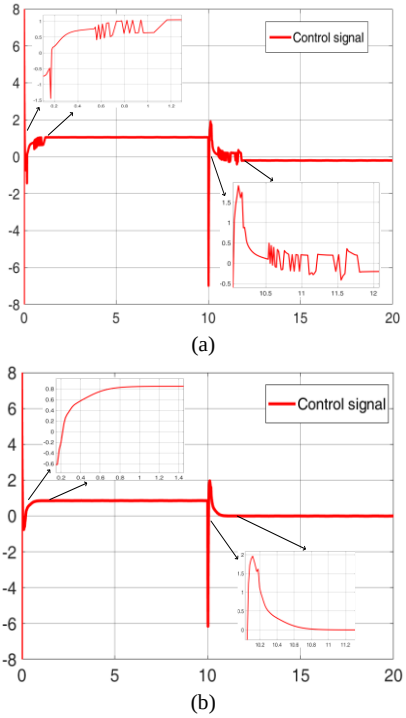

Fig. 3. Solution for chattering phenomenon, a) Method without $\eta|s|^{\lambda}$sign(s). b) Method with $\eta|s|^{\lambda}$sign(s)

Then formula (14) and formula (19) are rewritten as (20) and (21).

C. Simulation results

In this section, we have successfully designed a sliding mode controller for position control and attitude control of quadcopter based on Lyapunov stability theory. The chattering phenomenon reduction is also considered. In the next section, this controller will be used for quadcopter trajectory tracking and landing with the parameters shown in Table I.

$$\begin{bmatrix} U_x \\ U_y \\ U_z \end{bmatrix} = \begin{bmatrix} \frac{1}{c_2}(-c_1(x_2 - \dot{x_{1d}}) - c_2(h_1 x_2 - \ddot{x_{1d}}) - k_1 s_1 - \eta_1 |s_1|^{\lambda} sign(s_1)) \\ \frac{1}{c_4}(-c_3(x_4 - \dot{x_{3d}}) - c_4(h_3 x_4 - \ddot{x_{3d}}) - k_3 s_3 - \eta_3 |s_3|^{\lambda} sign(s_3)) \\ \frac{1}{c_6}(-c_5(x_6 - \dot{x_{5d}}) + c_6(h_5 x_6 - \ddot{x_{5d}}) - k_5 s_5 - \eta_5 |s_5|^{\lambda} sign(s_5)) \end{bmatrix} \quad (20)$$

$$\begin{bmatrix} U_2 \\ U_3 \\ U_4 \end{bmatrix} = \begin{bmatrix} \frac{1}{c_8 h_9}[-c_7(x_8 - \dot{x_{7d}}) - c_8(h_7 x_{10} x_{12} + h_8 x_{10} - \ddot{x_{7d}}) - k_7 s_7 - \eta_7 |s_7|^{\lambda} sign(s_7)] \\ \frac{1}{c_{10} h_{13}}[-c_9(x_{10} - \dot{x_{9d}}) - c_{10}(h_{11} x_8 x_{12} + h_{12} x_8 - \ddot{x_{9d}}) - k_9 s_9 - \eta_9 |s_9|^{\lambda} sign(s_9)] \\ \frac{1}{c_{12} h_{16}}[-c_{11}(x_{12} - \dot{x_{11d}}) - c_{12}(h_{15} x_8 x_{10} - \ddot{x_{11d}}) - k_{11} s_{11} - \eta_{11} |s_{11}|^{\lambda} sign(s_{11})] \end{bmatrix} \quad (21)$$

TABLE I. QUADCOPTER SIMULATION PARAMETERS

Parameters	Value	Unit	Desc
g	9.81	m/s^2	Gravitational acceleration
l	0.225	m	Distance from quadrotor center to rotor center
m	2	kg	Quadrotor mass
I_{xx}	0.0035	kg/m^2	Moment of inertia of the frame along the x axis.
I_{yy}	0.0035	kg/m^2	Moment of inertia of the frame along the y axis
I_{zz}	0.0050	kg/m^2	Moment of inertia of the frame along the z axis.

Fig. 4 and Fig. 5 are the simulation results of the output signals of the quadcopter's state variables. Based on the simulation results, we can see that external disturbances greatly influence the operation of the quadcopter. So, it is necessary to come up with a solution to resist these types of interference and make the quadcopter's operation smoother. Fig. 4 shows the output status signal of the system when the SMC controller is not used. It shows that the flight process is volatile when affected by interference. The simulation results in Fig. 5 show that when using the SMC controller for the above system, the orbital tracking quality of the quadcopter is better, and the stability is greatly improved.

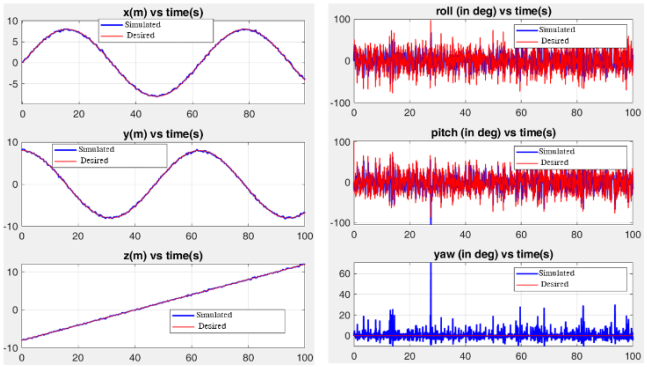

Fig. 4. When external disturbances without using the SMC controller

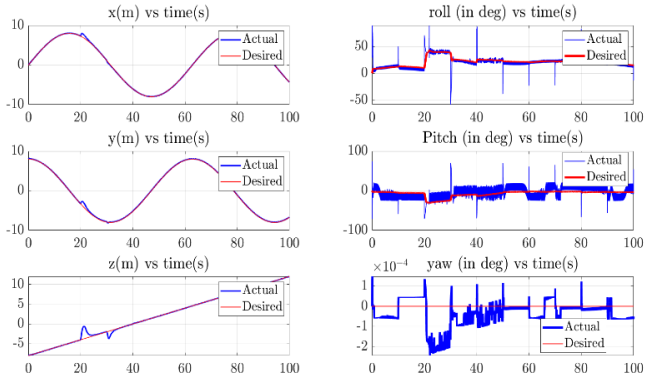

Fig. 5. When there is an external disturbance, the SMC controller is used

IV. LANDING CONTROL BASED ON ENERGY PREDICTION

We set up the simulation environment of the quadcopter in 3D space (20, 20, 16). Our simulation scenarios include:

Scenario 1: The quadcopter works in normal mode, meaning that its energy is full throughout the operation.

Scenario 2: During operation, bad weather, such as strong winds, requires more energy, causing the quadcopter to no longer have enough to reach the desired destination. It needs to land at a backup charging station to charge until the SoC reaches more than 90% and then continue flying to the desired destination.

The quadcopter flight process has two phases; phase 1 is when the quadcopter follows the trajectory to the desired location according to the GPS signal. Phase 2 is activated when the quadcopter detects the marker. Once the marker is detected, the quadcopter will land based on the error between the current position of the UAV and the marker based on computer vision technology. The quadcopter's landing process depends on energy prediction to avoid risks to the quadcopter. The entire flight and landing process of the quadcopter is carried out according to the algorithm flowchart in Fig. 6.

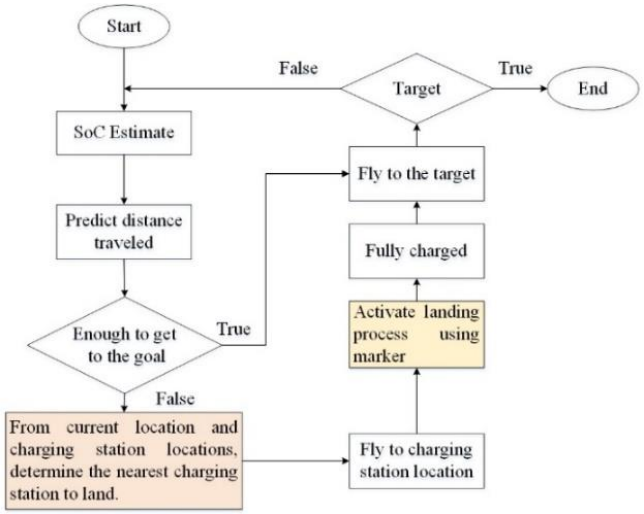

Fig. 6. Quadcopter flight algorithm flowchart based on energy prediction

Apply the controller built in section 3. Now, we apply to control the quadcopter to follow the trajectory based on the forecast of energy consumption. The SoC value of the battery is updated and monitored in real-time. From there, the algorithm will estimate the distance the quadcopter can travel. If the estimated distance is greater than or equal to the distance to the destination, the quadcopter will operate in mode 1. If the estimated distance is less than the distance to the destination, the quadcopter will activate mode 2 in Fig. 7. The algorithm to find the nearest landing station is activated. When the nearest landing station is found, the quadcopter will create a new trajectory to move there using the SMC controller to follow this new trajectory.

When $SoC < SoC_{threshold}$, UAV has not reached the target: $SoC < SoC_{threshold}$ UAV will the emergency landing mode be activated, and then the UAV will calculate and find the nearest landing station. The activation of the nearest station finding algorithm is completely random without any fixed point.

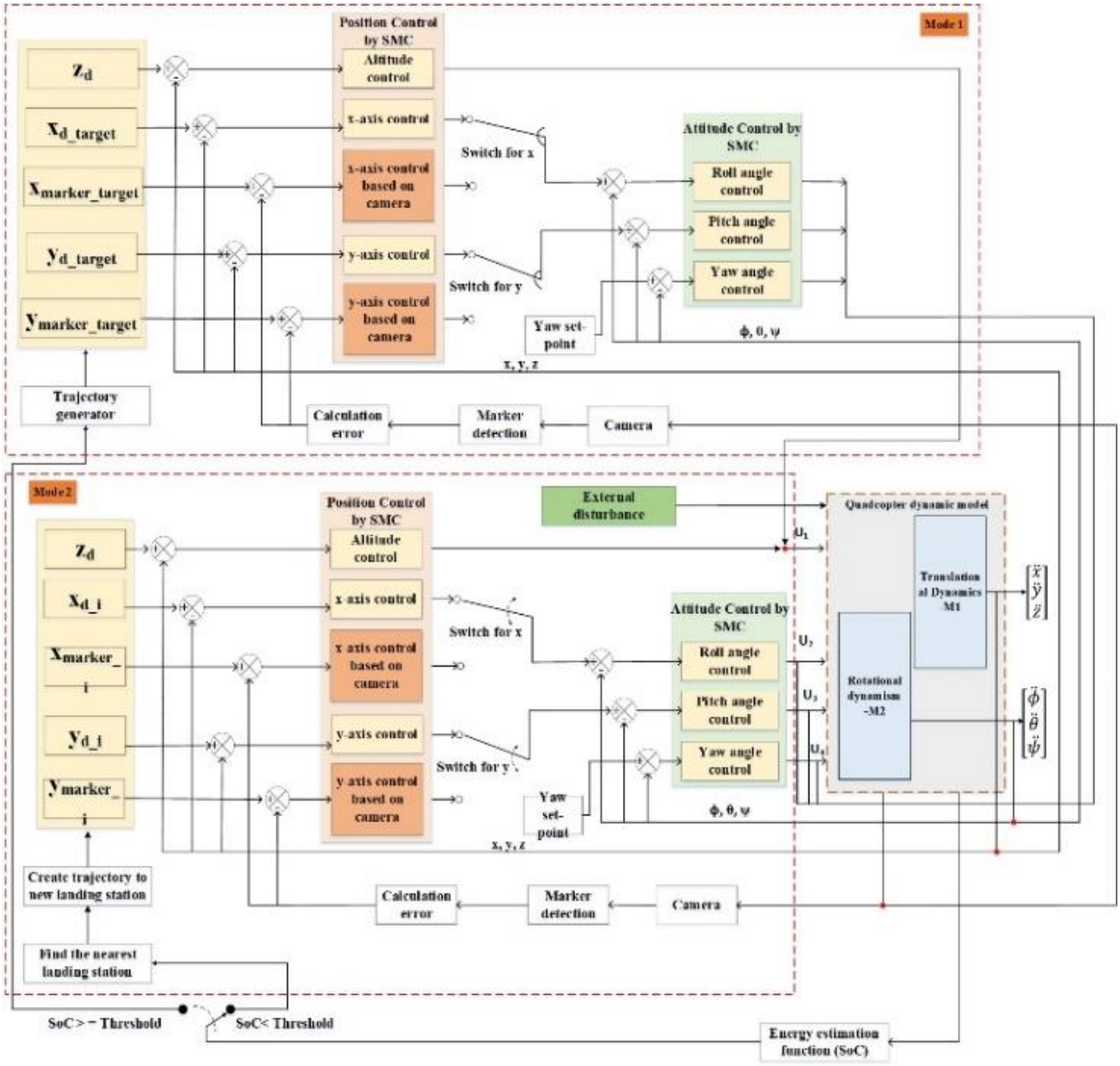

Fig. 7. Marker landing control scheme based on energy prediction

Below are some cases of UAV emergency landing when the energy is no longer enough to fly to the target as originally proposed. We have the positions of 3 markers in space, which are respectively 3 UAV landing stations with coordinates: maker1(10; 0; 0); maker2 (20; 10; 0); marker3 (20; 20; 0). Markers 1 and 2 are backup landing stations (charging stations), and marker 3 is the target landing station the UAV needs to reach during operation as shown in Fig. 8.

Scenario 1: The quadcopter works in normal mode, meaning that its energy is full throughout the operation.

This is a scenario where the UAV operates in normal mode under clear weather conditions, with no unusual power usage. The UAV flies in a pre-set trajectory using the SMC controller in mode 1 in Fig. 7.

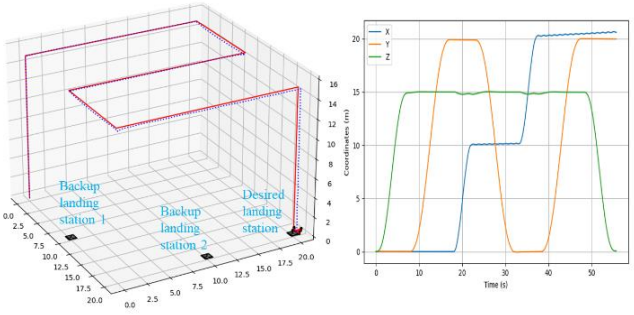

Fig. 8. When SoC ≥ $SoC_{threshold}$ UAV reaches the target

Scenario 2: UAVs work in bad weather conditions, such as strong winds and heavy rain, and therefore require more energy. Causing the quadcopter to no longer have enough to reach the desired destination. It needs to land at a backup charging station to charge until the SoC reaches more than 90% and then continue flying to the desired destination.

Distance from UAV→ marker:

$$S_i^q = \sqrt{(x_q - x_{maker}^i)^2 + (y_q - y_{maker}^i)^2 + (z_q - z_{maker}^i)^2} \quad (22)$$

$$S_{min} = min\{S_i^q\}, i = 1,2,..n \quad (23)$$

When the UAV flies to position A (0; 9.584; 15.004), it is predicted that its energy is not enough to fly to the destination. Therefore, it activates the emergency landing algorithm and goes to the nearest charging station to charge more energy until the SoC reaches 90%. Then, the UAV automatically takes off according to the given trajectory to reach the destination.

According to formula (22) and (23), the closest distance from position A to marker 1 is. The simulation results also show that the UAV landed at marker 1, as shown in Fig. 9.

Similarly, in Fig. 10, the UAV flies to position B (10.01; 3.94; 15) and is predicted to have insufficient energy to reach the target point. Therefore, it activates mode 2 in Fig. 7 and finds the closest distance to land at marker station 1.

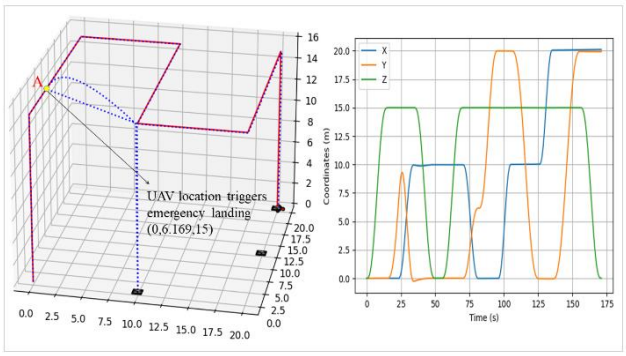

Fig. 9. When the UAV reaches A (0; 6.169; 15), it is predicted that it is running out of energy and needs to make an emergency landing

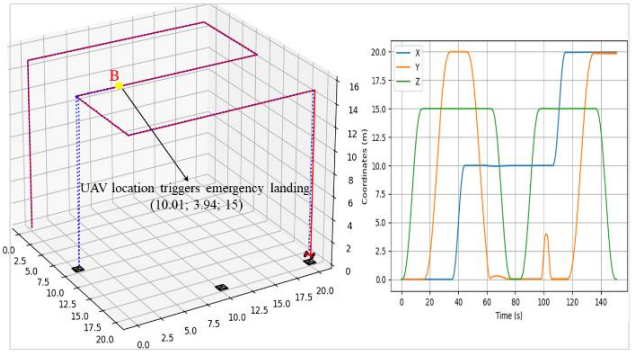

Fig. 10. When the UAV reaches B (10.01; 3.94; 15), it is predicted that it is running out of energy and needs to make an emergency landing

Fig. 11 shows that when the UAV flies to position C (10.01; 11.1; 15.0), the UAV is predicted not to have enough energy to reach the destination. Therefore, the mode to find the nearest charging station and make an emergency landing (mode 2 in Fig. 7) is activated at position C. When the battery's SoC reaches 90%, the UAV automatically takes off. It flies to the destination according to the predetermined trajectory.

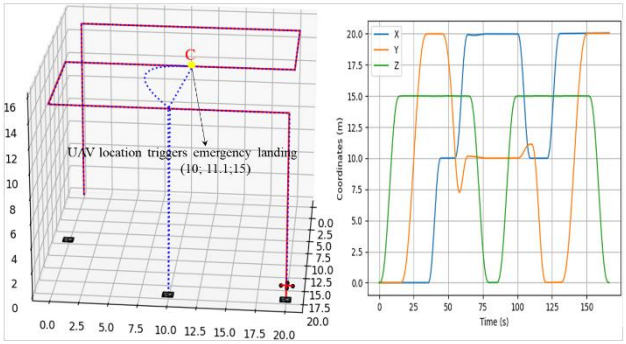

Fig. 11. When the UAV reaches C (10; 11.1; 15), it is predicted that it is running out of energy and needs to make an emergency landing

Similar to the above cases, the UAV flies to position D (20, 7.7, 15) and activates mode 2 in the diagram in Fig. 7. The algorithm finds marker 2 with the closest distance to the UAV, so the UAV lands at marker 2, as shown in Fig. 12.

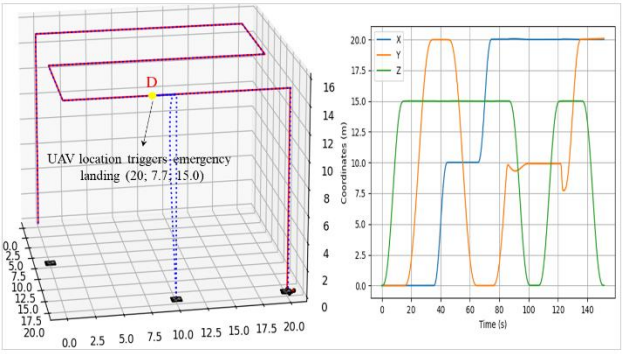

Fig. 12. When the UAV reaches D (20; 7.7; 15), it is predicted that it is running out of energy and needs to make an emergency landing

V. EXPEERIMENTAL RESULTS

In this study, we have only conducted experiments with the quadcopter's trajectory-tracking ability when using SMC and PID controllers. To experimentally verify the control algorithm, we tested the F450 quadcopter's ability to fly according to a given trajectory automatically in a real environment. The parameters of quadcopter F450 are given in Table II.

We simulate a space with dimensions of 20m wide, 20m long, and 20m high. In Fig. 14 and Fig. 15, the blue line is the desired trajectory and is loaded into the quadcopter's memory.

TABLE II. QUADCOPTER SIMULATION PARAMETERS

Parameters	Values
Mass	2.3 kg
Maximum current per motor	I_{motor}= 4.28 A
Current of other loads on the UAV	I_{other}= 6.2 A
Serial cell number in PIN	N_{series}= 3s Cell
Nominal voltage of the PIN	$V_{bat\ nominal}$ = 11.1 V
Battery capacity	Q= 4200 mmAh
Battery C-rate	C_{rate}=10
Battery discharge rule	DR = 80 %
Flying load	L_{flying}= 30 %

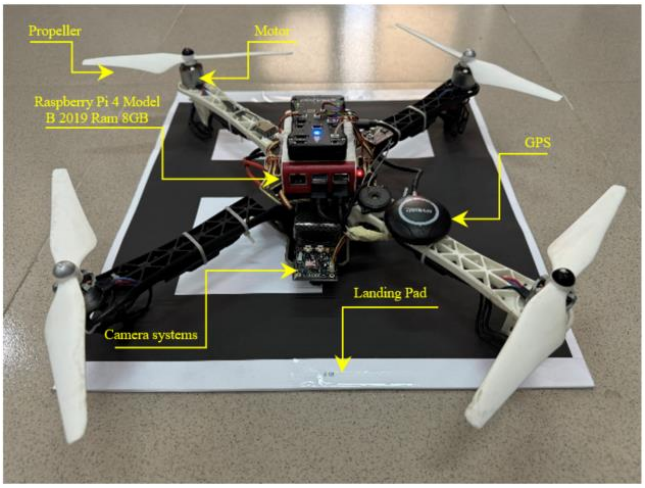

Fig. 13. Quadcopter F450

The orange line is the flight trajectory performed using the PID algorithm. The green line is the flight trajectory performed using the proposed SMC algorithm.

Fig. 14. Experimental results based on GPS data

All were carried out under the same environmental conditions of no rain and light wind. Looking at the trajectory data returned from the actual flight process in Fig. 14, we can see that using the PID algorithm gives much poorer trajectory control quality than the SMC algorithm we propose.

Table III lists the maximum trajectory tracking error in the x, y, and z directions of the quadcopter during the test corresponding to stages E1 to E7. From this table, we can see that the maximum trajectory tracking error in general in all directions of the SMC is always less than or equal to that of the PID controller.

The test scenario with the flight trajectory is as follows: from the starting point, the quadcopter flies vertically to a height of 15m at a speed of 2.05m/s, then maintains the same altitude and x direction, flies forward in the y direction for 20m at a speed of 1.01m/s; then maintains the same altitude and y direction, flies forward in the x direction for 10m at a speed of 1.01m/s; then maintains the same altitude and x direction, flies back in the y direction for 20m at a speed of 1.21m/s; then maintains the same altitude and y direction, flies forward in the x direction for 10m at a speed of 0.73m/s; then maintains the same altitude and x direction, flies forward in the y direction for 20m at a speed of 1.21m/s; Finally keep x and y directions constant and land at 0.59m/s.

TABLE III. ERRORS IN DIFFERENT DIRECTION DURING THE QUADCOPTER TEST FLIGHT

Stage	Error_x(m)		Error_y(m)		Error_z(m)	
	PID	SMC	PID	SMC	PID	SMC
E1(z)	0.15	0.15	1.75	0.5	2	1.5
E2(y)	0.75	0.4	1.5	1.0	0.1	0.1
E3(x)	0.75	0.1	0.75	0.75	0.1	0.1
E4(y)	0.5	0.5	1.0	0.75	0.1	0.1
E5(x)	1.75	0.75	2.0	1.4	0.1	0.1
E6(y)	0.5	0.25	2.0	1.6	0.1	0.1
E7(z)	0.75	0.5	1.0	0.5	3	0.6

E1: At the starting point, the quadcopter, keeping the x and y directions the same, flies vertically in the z direction to a height of 15m at a speed of 1.55m/s.
E2: Keeping the z and x directions the same, flies forward in the y direction 20m at a speed of 1.01m/s;
E3: Keeping the z and y directions the same, flies forward in the x direction 10m at a speed of 1.01m/s.
E4: Keeping the z and x directions the same, flies backward in the y direction 20m at a speed of 1.24m/s.
E5: Keeping the z and y directions the same, flies forward in the x direction 10m at a speed of 0.73m/s.
E6: Keeping the z and x directions the same, flies forward in the y direction 20m at a speed of 1.21m/s.
E7: Keeping x and y directions constant, land in the z-direction to the parking point at a speed of 0.59m/s.

Fig. 15. The position of the quadcopter in the x direction corresponds to three cases: desired trajectory, PID-controlled trajectory, and sliding mode control trajectory

More specifically, as shown in Fig. 15 and Table III, the trajectory tracking error in the x direction in stage E1 has a relatively small and similar value, about 0.15m, for both PID and sliding controllers. Next, stage E2's largest trajectory tracking error in the x direction is 0.4m for the sliding control and 0.75m for the PID control. In stage E3, the trajectory tracking error of the PID controller tends to increase to 0.75m at the end of the stage, while the sliding controller gives a trajectory tracking error of 0.1m. In stage E4, the largest trajectory tracking error in the x direction of the sliding control and PID is almost equal to 0.5m. In stage E5, the largest trajectory tracking error in the x direction is 1.75m for the PID and 0.75m for the sliding controller. The E6 phase has the largest error of 0.5m for the PID controller and 0.25m for the glide control. The landing phase, E7, has the largest trajectory tracking error of the glide control of 0.5m and 0.75m for the glide and PID controllers, respectively.

Fig. 16 shows that the trajectory tracking stability control quality of the sliding mode controller is better than that of the PID control, especially during the stationary stability process at the y-direction position.

In Fig. 16 and the data in Table III, the E1 stage has the largest y-direction error for the PID controller at 1.75m, while the SMC remains stable in the y-direction with a maximum error of 0.5m. Next, in the E2 stage, the quadcopter moves forward in the y-direction for 20m; at this time, the largest y-direction tracking error of the PID controller is 1.5m and 1m for the SMC. In the E3 stage, the largest y-direction tracking error is 0.75m for both controllers. In the E4 stage, the largest y-direction tracking error is 1m for the PID controller and 0.75m for the SMC. In the next E5 stage, the PID controller has the largest tracking error of 2m, while the SMC controller has 1.4m. In stage E6, this error is 2m for the PID controller and 1.6m for the glide controller. In stage E7, the landing stage, the maximum y-direction tracking error of the PID is 1m, while for the SMC, this error is 0.5m.

The position of the quadcopter in the z direction and the position error in the z direction are shown in Fig. 17 and Table III. The z-direction is kept stable at the height of 15m in stages E2, E3, E4, E5, E6, and changes in stages E1 and E7. During the altitude holding stages, the maximum errors of the PID controller and the SMC are similar and equal to 0.1m. However, during the take-off stage E1, the maximum position tracking error in the z direction of the PID controller is approximately 2m and is 1.5m for the SMC. During the landing stage E7, these errors are 3m and 0.6m for the PID controller and the SMC, respectively.

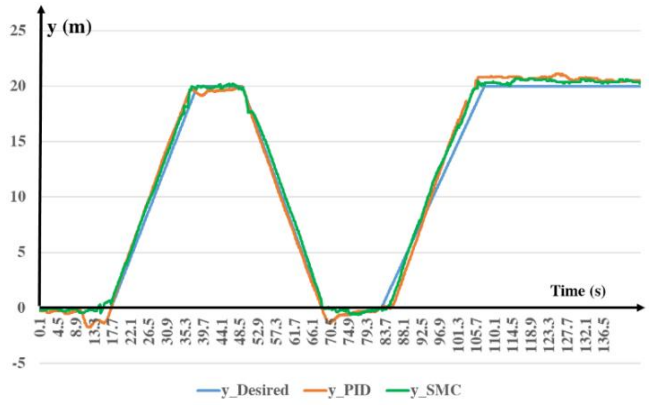

Fig. 16. The position of the quadcopter in the y direction corresponds to three cases: desired trajectory, PID-controlled trajectory, and sliding mode control trajectory

Fig. 17. The position of the quadcopter in the z direction corresponds to three cases: desired trajectory, PID-controlled trajectory, and sliding mode control trajectory

VI. CONCLUSIONS

In this paper, the sliding mode control (SMC) controller is used to control the position and attitude of the quadcopter. Firstly, the dynamic model of the quadcopter is introduced and fully constructed under the consideration of external disturbances. Then, the controller is proposed and developed. The SMC controller is built based on the Lyapunov function so that the system's stability is mathematically guaranteed. The flight process of the quadcopter is carried out in two modes based on the real-time prediction of the quadcopter's energy consumption to avoid risks and support the quadcopter to complete the task under various conditions. The simulation results show the controller can achieve trajectory-tracking feedback with good accuracy and response time.

ACKNOWLEDGMENT

The author would like to thank Thai Nguyen University of Information and communication technology, Viet Nam.

REFERENCES

[1] J. Wu *et al*., "An Adaptive Conversion Speed Q-Learning Algorithm for Search and Rescue UAV Path Planning in Unknown Environments," *IEEE Transactions on Vehicular Technology*, vol. 72, no. 12, pp. 15391–15404, Dec. 2023, doi: 10.1109/tvt.2023.3297837.

[2] C. Zhang, W. Zhou, W. Qin, and W. Tang, "A novel UAV path planning approach: Heuristic crossing search and rescue optimization algorithm," *Expert Systems with Applications*, vol. 215, p. 119243, Apr. 2023, doi: 10.1016/j.eswa.2022.119243.

[3] M. Song, Y. Huo, Z. Liang, X. Dong, and T. Lu, "UAV Communication Recovery under Meteorological Conditions," *Drones*, vol. 7, no. 7, p. 423, Jun. 2023, doi: 10.3390/drones7070423.

[4] O. Kozlov, Y. Kondratenko, and O. Skakodub, "Intelligent IoT-based Control System of the UAV for Meteorological Measurements," *Journal of Mobile Multimedia*, pp. 555–596, May 2024, doi: 10.13052/jmm1550-4646.2032.

[5] C. Mourgelas, E. Micha, E. Chatzistavrakis, and I. Voyiatzis, "Classification of Unmanned Aerial Vehicles in Meteorology: A Survey," *Environmental Sciences Proceedings*, vol. 26, no. 1, p. 135, Aug. 2023, doi: 10.3390/environsciproc2023026135.

[6] J. Peng *et al*., "Near Surface Layer Meteorological Observation System Based on Programmable Unmanned Aerial Vehicles," *Journal of Physics: Conference Series*, vol. 2419, no. 1, p. 012099, Jan. 2023, doi: 10.1088/1742-6596/2419/1/012099.

[7] M. Aljohani, R. Mukkamala, and S. Olariu, "Autonomous Strike UAVs in Support of Homeland Security Missions: Challenges and Preliminary Solutions," *IEEE Access*, vol. 12, pp. 90979-90996, 2024, doi: 10.1109/access.2024.3420235.

[8] P. Daponte and F. Paladi, "Monitoring and Protection of Critical Infrastructure by Unmanned Systems," *NATO Science for Peace and Security Series - D: Information and Communication Security*, vol. 63, pp. 1-238, Jan. 2023, doi: 10.3233/nicsp63.

[9] F. Outay, H. A. Mengash, and M. Adnan, "Applications of unmanned aerial vehicle (UAV) in road safety, traffic and highway infrastructure management: Recent advances and challenges," *Transportation Research Part A: Policy and Practice*, vol. 141, pp. 116–129, Nov. 2020, doi: 10.1016/j.tra.2020.09.018.

[10] S. Feroz and S. Abu Dabous, "UAV-Based Remote Sensing Applications for Bridge Condition Assessment," *Remote Sensing*, vol. 13, no. 9, p. 1809, May 2021, doi: 10.3390/rs13091809.

[11] X. Kong, C. Ni, G. Duan, G. Shen, Y. Yang, and S. K. Das, "Energy Consumption Optimization of UAV-Assisted Traffic Monitoring Scheme With Tiny Reinforcement Learning," *IEEE Internet of Things Journal*, vol. 11, no. 12, pp. 21135–21145, Jun. 2024, doi: 10.1109/jiot.2024.3365293.

[12] S. Ali, A. Jalal, M. Hamad Alatiyyah, K. Alnowaiser, and J. Park, "Vehicle Detection and Tracking in UAV Imagery via YOLOv3 and Kalman Filter," *Computers, Materials & Continua*, vol. 76, no. 1, pp. 1249–1265, 2023, doi: 10.32604/cmc.2023.038114.

[13] S. Emmanuel and P. U. Emmoh, "Enhancing Traffic Management in Urban Areas through UAV-Assisted Intelligent Mobile Systems," *Journal of Networking and Communication Systems (JNACS)*, vol. 7, no. 1, pp. 17–27, 2024, doi: 10.46253/jnacs.v7i1.a2.

[14] M. Hanzla, S. Ali, and A. Jalal, "Smart Traffic Monitoring through Drone Images via Yolov5 and Kalman Filter," *2024 5th International Conference on Advancements in Computational Sciences (ICACS)*, pp. 1-8, Feb. 2024, doi: 10.1109/icacs60934.2024.10473259.

[15] X. Kong, C. Ni, G. Duan, G. Shen, Y. Yang, and S. K. Das, "Energy Consumption Optimization of UAV-Assisted Traffic Monitoring Scheme With Tiny Reinforcement Learning," *IEEE Internet of Things Journal*, vol. 11, no. 12, pp. 21135–21145, Jun. 2024, doi: 10.1109/jiot.2024.3365293.

[16] D. Lu, J. Ye, Y. Wang, and Z. Yu, "Plant Detection and Counting: Enhancing Precision Agriculture in UAV and General Scenes," *IEEE Access*, vol. 11, pp. 116196–116205, 2023, doi: 10.1109/access.2023.3325747.

[17] R. I. Mukhamediev *et al*., "Coverage Path Planning Optimization of Heterogeneous UAVs Group for Precision Agriculture," *IEEE Access*, vol. 11, pp. 5789–5803, 2023, doi: 10.1109/access.2023.3235207.

[18] N. Delavarpour, C. Koparan, J. Nowatzki, S. Bajwa, and X. Sun, "A Technical Study on UAV Characteristics for Precision Agriculture Applications and Associated Practical Challenges," *Remote Sensing*, vol. 13, no. 6, p. 1204, Mar. 2021, doi: 10.3390/rs13061204.

[19] P. Velusamy, S. Rajendran, R. K. Mahendran, S. Naseer, M. Shafiq, and J.-G. Choi, "Unmanned Aerial Vehicles (UAV) in Precision Agriculture: Applications and Challenges," *Energies*, vol. 15, no. 1, p. 217, Dec. 2021, doi: 10.3390/en15010217.

[20] A. Lambertini, E. Mandanici, M. A. Tini, and L. Vittuari, "Technical Challenges for Multi-Temporal and Multi-Sensor Image Processing Surveyed by UAV for Mapping and Monitoring in Precision Agriculture," *Remote Sensing*, vol. 14, no. 19, p. 4954, Oct. 2022, doi: 10.3390/rs14194954.

[21] H. Shakhatreh *et al*., "Unmanned Aerial Vehicles (UAVs): A Survey on Civil Applications and Key Research Challenges," *IEEE Access*, vol. 7, pp. 48572–48634, 2019, doi: 10.1109/access.2019.2909530.

[22] M. Krichen and A. Mihoub, "Unmanned Aerial Vehicles Communications Security Challenges: A Survey," *Synthesis Lectures on Intelligent Technologies*, pp. 349–373, 2023, doi: 10.1007/978-3-031-32037-8_12.

[23] A. S. Prasetia, R.-J. Wai, Y.-L. Wen, and Y.-K. Wang, "Mission-Based Energy Consumption Prediction of Multirotor UAV," *IEEE Access*, vol. 7, pp. 33055–33063, 2019, doi: 10.1109/access.2019.2903644.

[24] L. H. Manjarrez, J. C. Ramos-Fernández, E. S. Espinoza, and R. Lozano, "Estimation of Energy Consumption and Flight Time Margin for a UAV Mission Based on Fuzzy Systems," *Technologies*, vol. 11, no. 1, p. 12, Jan. 2023, doi: 10.3390/technologies11010012.

[25] M. Suwe, M. Eigenseer, and C. Werner, "Model-Based Evaluation of Energy Systems for Multirotor UAV Based on Batteries and Fuel Cells," *Journal of Aviation Technology and Engineering*, vol. 12, no. 1, Feb. 2023, doi: 10.7771/2159-6670.1262.

[26] S. A. H. Mohsan, N. Q. H. Othman, Y. Li, M. H. Alsharif, and M. A. Khan, "Unmanned aerial vehicles (UAVs): practical aspects, applications, open challenges, security issues, and future trends," *Intelligent Service Robotics*, vol. 16, no. 1, pp. 109-137, Jan. 2023, doi: 10.1007/s11370-022-00452-4.

[27] A. Baharuddin and M. A. Mohd Basri, "Trajectory Tracking of a Quadcopter UAV using PID Controller," *ELEKTRIKA- Journal of Electrical Engineering*, vol. 22, no. 2, pp. 14–21, Aug. 2023, doi: 10.11113/elektrika.v22n2.440.

[28] W. Altalabani and Y. Alaiwi, "Optimized Adaptive PID Controller Design for Trajectory Tracking of a Quadcopter," *Mathematical Modelling of Engineering Problems*, vol. 9, no. 6, pp. 1490–1496, Dec. 2022, doi: 10.18280/mmep.090607.

[29] S. Abdelhay and A. Zakriti, "Modeling of a Quadcopter Trajectory Tracking System Using PID Controller," *Procedia Manufacturing*, vol. 32, pp. 564–571, 2019, doi: 10.1016/j.promfg.2019.02.253.

[30] J. Yoon and J. Doh, "Optimal PID control for hovering stabilization of quadcopter using long short term memory," *Advanced Engineering Informatics*, vol. 53, p. 101679, Aug. 2022, doi: 10.1016/j.aei.2022.101679.

[31] A. Belmouhoub, S. Medjmadj, Y. Bouzid, S. H. Derrouaoui, and M. Guiatni, "Enhanced backstepping control for an unconventional quadrotor under external disturbances," *The Aeronautical Journal*, vol. 127, no. 1310, pp. 627–650, Jul. 2022, doi: 10.1017/aer.2022.72.

[32] Y. Nettari, S. Kurt, and M. Labbadi, "Adaptive Robust Control based on Backstepping Sliding Mode techniques for Quadrotor UAV under external disturbances," *IFAC-PapersOnLine*, vol. 55, no. 12, pp. 252–257, 2022, doi: 10.1016/j.ifacol.2022.07.320.

[33] W. Xie, D. Cabecinhas, R. Cunha, and C. Silvestre, "Adaptive Backstepping Control of a Quadcopter With Uncertain Vehicle Mass, Moment of Inertia, and Disturbances," *IEEE Transactions on Industrial Electronics*, vol. 69, no. 1, pp. 549–559, Jan. 2022, doi: 10.1109/tie.2021.3055181.

[34] W. Xie, W. Zhang, and C. Silvestre, "Saturated Backstepping-Based Tracking Control of a Quadrotor With Uncertain Vehicle Parameters and External Disturbances," *IEEE Control Systems Letters*, vol. 6, pp. 1634–1639, 2022, doi: 10.1109/lcsys.2021.3129891.

[35] H. Pang, R. Yao, P. Wang, and Z. Xu, "Adaptive backstepping robust tracking control for stabilizing lateral dynamics of electric vehicles with uncertain parameters and external disturbances," *Control Engineering Practice*, vol. 110, p. 104781, May 2021, doi: 10.1016/j.conengprac.2021.104781.

[36] A. Eltayeb, M. F. Rahmat, M. A. M. Basri, M. A. M. Eltoum, and M. S. Mahmoud, "Integral Adaptive Sliding Mode Control for Quadcopter UAV Under Variable Payload and Disturbance," *IEEE Access*, vol. 10, pp. 94754–94764, 2022, doi: 10.1109/access.2022.3203058.

[37] N. P. Nguyen and P. Pitakwachara, "Integral terminal sliding mode fault tolerant control of quadcopter UAV systems," *Scientific Reports*, vol. 14, no. 1, May 2024, doi: 10.1038/s41598-024-61273-2.

[38] J. Chaoraingern, V. Tipsuwanporn, and A. Numsomran, "Modified Adaptive Sliding Mode Control for Trajectory Tracking of Mini-drone Quadcopter Unmanned Aerial Vehicle," *International Journal of Intelligent Engineering and Systems*, vol. 13, no. 5, pp. 145–158, Oct. 2020, doi: 10.22266/ijies2020.1031.14.

[39] E. Ahmed, "Robust Adaptive Sliding Mode Control Design for Quadrotor Unmanned Aerial Vehicle Trajectory Tracking," *International Journal of Computing and Digital Systems*, vol. 9, no. 2, pp. 249–257, Jan. 2020, doi: 10.12785/ijcds/090210.

[40] H. T. Sekban and A. Basci, "Designing New Model-Based Adaptive Sliding Mode Controllers for Trajectory Tracking Control of an Unmanned Ground Vehicle," *IEEE Access*, vol. 11, pp. 101387–101397, 2023, doi: 10.1109/access.2023.3313942.

[41] B. Ma, W. Pei, and Q. Zhang, "Trajectory Tracking Control of Autonomous Vehicles Based on an Improved Sliding Mode Control Scheme," *Electronics*, vol. 12, no. 12, p. 2748, Jun. 2023, doi: 10.3390/electronics12122748.

[42] N. P. Nguyen, N. X. Mung, H. L. N. N. Thanh, T. T. Huynh, N. T. Lam, and S. K. Hong, "Adaptive Sliding Mode Control for Attitude and Altitude System of a Quadcopter UAV via Neural Network," *IEEE Access*, vol. 9, pp. 40076–40085, 2021, doi: 10.1109/access.2021.3064883.

[43] J. Rao, B. Li, Z. Zhang, D. Chen, and W. Giernacki, "Position Control of Quadrotor UAV Based on Cascade Fuzzy Neural Network," *Energies*, vol. 15, no. 5, p. 1763, Feb. 2022, doi: 10.3390/en15051763.

[44] K. Jia, S. Lin, Y. Du, C. Zou, and M. Lu, "Research on Route Tracking Controller of Quadrotor UAV Based on Fuzzy Logic and RBF Neural Network," *IEEE Access*, vol. 11, pp. 111433–111447, 2023, doi: 10.1109/access.2023.3322944.

[45] B. Jiang, B. Li, W. Zhou, L.-Y. Lo, C.-K. Chen, and C.-Y. Wen, "Neural Network Based Model Predictive Control for a Quadrotor UAV," *Aerospace*, vol. 9, no. 8, p. 460, Aug. 2022, doi: 10.3390/aerospace9080460.

[46] J. Morales, I. Castelo, R. Serra, P. U. Lima, and M. Basiri, "Vision-Based Autonomous Following of a Moving Platform and Landing for an Unmanned Aerial Vehicle," *Sensors*, vol. 23, no. 2, p. 829, Jan. 2023, doi: 10.3390/s23020829.

[47] M. F. Khyasudeen *et al*., "The development of a GPS-based autonomous quadcopter towards precision landing on moving platform," *International Journal of Vehicle Autonomous Systems*, vol. 16, pp. 108–126, 2022, doi: 10.1504/ijvas.2022.133006.

[48] I. S. Amiri *et al*., "The development of a GPS-based autonomous quadcopter for precision landing on a moving platform," *International Journal of Vehicle Autonomous Systems*, vol. 1, no. 1, 2021, doi: 10.1504/ijvas.2021.10055418.

[49] A. S. Priambodo, F. Arifin, A. Nasuha, Muslikhin, and A. Winursito, "A Vision and GPS Based System for Autonomous Precision Vertical Landing of UAV Quadcopter," *Journal of Physics: Conference Series*, vol. 2406, no. 1, p. 012004, Dec. 2022, doi: 10.1088/1742-6596/2406/1/012004.

[50] J. Wubben *et al*., "A vision-based system for autonomous vertical landing of unmanned aerial vehicles," *2019 IEEE/ACM 23rd International Symposium on Distributed Simulation and Real Time Applications (DS-RT)*, pp. 1-7, Oct. 2019, doi: 10.1109/ds-rt47707.2019.8958701.

[51] L. Xin, Z. Tang, W. Gai, and H. Liu, "Vision-Based Autonomous Landing for the UAV: A Review," *Aerospace*, vol. 9, no. 11, p. 634, Oct. 2022, doi: 10.3390/aerospace9110634.

[52] A. Khazetdinov, A. Zakiev, T. Tsoy, M. Svinin, and E. Magid, "Embedded ArUco: a novel approach for high precision UAV landing," *2021 International Siberian Conference on Control and Communications (SIBCON)*, pp. 1-6, May 2021, doi: 10.1109/sibcon50419.2021.9438855.

[53] A. Marut, K. Wojtowicz, and K. Falkowski, "ArUco markers pose estimation in UAV landing aid system," *2019 IEEE 5th International Workshop on Metrology for AeroSpace (MetroAeroSpace)*, pp. 261-266, Jun. 2019, doi: 10.1109/metroaerospace.2019.8869572.

[54] I. E. Sevostyanov and D. V. Devitt, "Uav Visual Positioning System For High-Precision Autonomous Landing," *Mathematical Methods in Technologies and Technics*, no. 7, pp. 83–86, 2021, doi: 10.52348/2712-8873_mmtt_2021_7_83.

[55] Z. Yue, H. Shuai, D. Xuechao, and X. Ziqi, "UAV Landing Aid Hexapod Robot based on ArUco Marker and Sparse Optical Flow," *Journal of Physics: Conference Series*, vol. 2281, no. 1, p. 012002, Jun. 2022, doi: 10.1088/1742-6596/2281/1/012002.

[56] C. V. Nguyen, H. T. Tran, H. T. Do, T. Hoang, D. L. T. Tran, and M. T. Nguyen, "A Novel Framework of Visual Detection, Tracking and Landing for UAVs Utilizing AR Markers," *2023 International Conference on Control, Robotics and Informatics (ICCRI)*, pp. 81-85, May 2023, doi: 10.1109/iccri58865.2023.00023.

[57] H.-H. Kang and S.-Y. Shin, "Precise Drone Landing System Using Aruco Maker," *The Journal of Korean Institute of Communications and Information Sciences*, vol. 47, no. 1, pp. 145–150, Jan. 2022, doi: 10.7840/kics.2022.47.1.145.

[58] L. B. Junior *et al*., "A Comparison of Fiducial Markers Pose Estimation for UAVs Indoor Precision Landing," *Optimization, Learning Algorithms and Applications*, pp. 18–33, 2024, doi: 10.1007/978-3-031-53025-8_2.

[59] F. Yacef, N. Rizoug, L. Degaa, and M. Hamerlain, "Energy-Efficiency Path Planning for Quadrotor UAV Under Wind Conditions," *2020 7th International Conference on Control, Decision and Information Technologies (CoDIT)*, vol. 1, pp. 1133-1138 Jun. 2020, doi: 10.1109/codit49905.2020.9263968.

[60] M. Shah Alam and J. Oluoch, "A survey of safe landing zone detection techniques for autonomous unmanned aerial vehicles (UAVs)," *Expert Systems with Applications*, vol. 179, p. 115091, Oct. 2021, doi: 10.1016/j.eswa.2021.115091.

[61] Z. Wang and G. Wang, "Energy-Efficient Mobile Edge Computing Assisted by Layered Uavs Based on Convex Optimization," *Physical Communication*, vol. 65, p. 102382, 2023, doi: 10.2139/ssrn.4576663.

[62] H. Jin *et al*., "A survey of energy efficient methods for UAV communication," *Vehicular Communications*, vol. 41, p. 100594, Jun. 2023, doi: 10.1016/j.vehcom.2023.100594.

[63] D. An, R. Krzysiak, D. Hollenbeck, and Y. Chen, "Battery-health-aware UAV mission planning using a cognitive battery management system," *2023 International Conference on Unmanned Aircraft Systems (ICUAS)*, pp. 523-528, Jun. 2023, doi: 10.1109/icuas57906.2023.10156138.

[64] B. Bose, S. Shaosen, W. Li, L. Gao, K. Wei, and A. Garg, "Cloud-Battery management system based health-aware battery fast charging architecture using error-correction strategy for electric vehicles," *Sustainable Energy, Grids and Networks*, vol. 36, p. 101197, Dec. 2023, doi: 10.1016/j.segan.2023.101197.

[65] I. Lebedev, A. Erashov, and A. Shabanova, "Accurate Autonomous UAV Landing Using Vision-Based Detection of ArUco-Marker," *Interactive Collaborative Robotics*, pp. 179–188, 2020, doi: 10.1007/978-3-030-60337-3_18.

[66] A. E. S. Morando, M. F. Santos, P. Castillo, and A. Correa-Victorino, "Vision-Based Algorithm for Autonomous Aerial Landing," *2024 International Conference on Unmanned Aircraft Systems (ICUAS)*, pp. 652-657, Jun. 2024, doi: 10.1109/icuas60882.2024.10556880.

[67] O. Gharsa, M. M. Touba, M. Boumehraz, N. Abderrahman, S. Bellili, and A. Titaouine, "Autonomous landing system for A Quadrotor using a vision-based approach," *2024 8th International Conference on Image and Signal Processing and their Applications (ISPA)*, pp. 1-5, Apr. 2024, doi: 10.1109/ispa59904.2024.10536784.

[68] G. G. Jin, P. Pal, Y. K. Chung, H. K. Kang, T. T. Yetayew, and S. Bhakta, "Modelling, control and development of GUI-based simulator for a quadcopter using nonlinear PID control," *Australian Journal of Electrical and Electronics Engineering*, vol. 20, no. 4, pp. 387–399, Aug. 2023, doi: 10.1080/1448837x.2023.2249166.